Microscopic investigation of the memory effect found in micropatterned nematic liquid crystal cells

Thet Naing Oo,* Yuuki Yasu, Munehiro Kimura, and Tadashi Akahane
Department of Electrical Engineering, Faculty of Engineering, Nagaoka University of Technology, 1603-1 Kamitomioka, Nagaoka, Niigata 940-2188, Japan

(Received 10 February 2007; revised manuscript received 11 May 2007; published 18 September 2007)

Isotropic untreated indium-tin-oxide layers can cause memory alignment of nematic liquid crystals. We have demonstrated an experimental method to characterize this effect by using a micropatterned surface. We tried to imprint a high tilt on an indium-tin-oxide substrate surface. We also investigated microscopic switching behavior of a memory-induced nematic liquid crystal cell by means of a vertical field effect.

DOI: 10.1103/PhysRevE.76.031705 PACS number(s): 61.30.Hn

I. INTRODUCTION

Several kinds of memory effects in liquid crystal (LC) cells have been reported and widely discussed thus far. They are interesting from the viewpoint of fundamental research as well as for improving the quality of existing LC display devices. These memory effects can be generally classified into two groups. The first group is concerned with surface memory effects (SME) without applying external fields [1–6]. Here, SME refers to the phenomenon wherein an initially isotropic surface can be rendered anisotropic by contact with an anisotropic medium. These were first reported by Friedel using isotropic glass in contact with anisotropic liquid crystals [1]. Clark discovered the same effect of LCs on polymer surfaces [2]. He found that by exposing a polymer surface to a smectic-*A* or -G phase of a LC, the multidomain texture of the smectic was imprinted on the polymer surface, inducing a similar defect texture in the nematic phase of the LC. The SME was further investigated by Ouchi *et al.* using optical second harmonic generation (SHG) and ellipsometry [3]. Their results showed that LC molecules appeared to have anchored to the memory-imprinted polymer surface with a considerable azimuthal anisotropy in their orientational distribution arising from reorientation in local surface potential wells by the bulk alignment. Moreover, Dreyfus-Lambez *et al.* studied the effects of memory-induced anchoring on a bare untreated indium-tin-oxide (ITO) substrate [4]. However, they did not succeed in imprinting a pretilt on the ITO substrate. In addition to these, Tsonev *et al.* and Petrov *et al.* elaborated the relationship between the nature of the surface coatings—conductive or dielectric—and SME [5,6].

The second group is concerned with memory effects under the influence of applied external fields. This type of memory effect maintains the field-induced orientation of LCs caused by external fields after the field is removed [7–14]. Sato *et al.* first reported such a memory effect in compensated LCs [7]. They observed that the memory effects depend on the surface conditions of tin-oxide-coated glass substrates and the applied electric field. Moreover, they found that the temperature range within which the memory effects occur is inversely proportional to the sample thickness. Therefore, a small sample thickness is needed to achieve the memory effects over a wide temperature range. The other example of these effects with application of external fields is the switching of LC alignment on a bistable surface [15,16]. Boyd *et al.* discovered a new class of nematic LC storage effects based on the elastic and topological bistability of the director orientation, and switching between bistable states was demonstrated using both electric and magnetic fields [15]. They have shown that disclinations, which is anathema to most LC devices, can serve useful functions when properly controlled. Moreover, Dozov *et al.* proposed a new kind of passive surface-controlled nematic display with bistable textures [16]. Switching by breaking surface anchoring is very fast and can be controlled by pulses of a few microseconds duration.

In the present paper, we demonstrate two kinds of memory effects by using a micropatterned surface. We have already proposed single-step laser patterning on a photoalignment layer using a photomask to achieve an equilibrium configuration of LC molecules in contact with a periodically patterned substrate [17–19]. The patterns were formed by stripes of alternating planar and homeotropic anchorings. This micropatterned surface provides two equilibrium states with equal energy minima. The purpose of this paper is to investigate memory alignment of nematic LCs on isotropic, untreated ITO substrates by imprinting a counter-alignment, i.e., a micropatterned alignment on the ITO surface. We also studied switching behavior of this memory-induced LC cell.

II. EXPERIMENT

A. Preparation of ITO-coated glass substrates

Two types of ITO-coated glasses were used. One was supplied by Nipon Seiki Co., Ltd. and the other by Corning Inc. The former ITO-coated glass (Nihon Seiki; hereafter abbreviated to ITO-NS) consisted of a 20-nm-thick ITO layer on a 1.1-mm-thick glass substrate, and the latter ITO-coated glass (Corning-1737F; hereafter abbreviated to ITO-CN) consisted of 60-nm-thick ITO on a 0.7-mm-thick glass substrate. ITO-coated glass substrates, with dimensions of 23×15 mm^2 (for fabrication of a sample cell) and 10×2.8 mm^2 [for atomic force microscopy (AFM) and scanning tunneling microscopy (STM) measurements], were washed with detergent and dis-

*tno2002@stn.nagaokaut.ac.jp

tilled water in an ultrasonic bath, followed by nitrogen blow-drying, and were then dried at 50 °C for 5 min.

B. Preparation of LC cells using bare untreated ITO

LC cells were constructed with two pieces of bare untreated ITO-coated substrates. The cells were filled with a nematic LC, 4′-*n*-pentyl-4-cyanobiphenyl (5CB supplied by Merck, Japan), by capillary action in the isotropic phase and gradually cooled down to room temperature. The properties of 5CB were as follows: nematic-isotropic phase transition temperature $T_{NI}=35.5$ °C, birefringence $\Delta n=0.182$ (at 25 °C, $\lambda=633$ nm), dielectric anisotropy $\Delta\varepsilon=+9.9$ (at 25 °C, 1 kHz), and elastic constants $K_{11}=7.1$ pN, $K_{22}=4.1$ pN, and $K_{33}=9.8$ pN (at 22 °C). Polarizing optical microscopy (POM; Nikon) was used to characterize the LC textures.

C. Micropatterned photoalignment of polyimide alignment films

Clean ITO-coated substrates (ITO-NS) were spin-coated with 2.5 wt. % polyimide PIA-1 solutions (Chisso Corp., Japan) at 800 rpm for 1 s and at 2200 rpm for 30 s, and the spin-cast substrates were then baked at 220 °C for 1 h for removing the solvent and for curing. The thickness of the PIA-1 films was about 10 nm. The alignment film PIA-1 promoted homeotropic alignment of nematic LCs. Micropatterning of the PIA-1 film was performed using a photomask (0.5 μm line and space) by means of a photoalignment technique [20]. We propose two types of geometries of the linearly polarized laser exposure, as shown in Figs. 1(a) and 1(b). In the type 1 exposure geometry, the photomask pattern was parallel to the polarization direction of the linearly polarized laser light, and in the type 2 exposure geometry, the photomask pattern was perpendicular to the polarization direction of the linearly polarized laser light. In this study, the type 2 exposure geometry was applied because this provides two domains with opposite tilt angles of the LC directors, and the equilibrium tilt angle in the bulk was nearly 45° in the two domains in the case of the infinite anchoring [17]. On the other hand, the type 1 exposure geometry provides two domains with opposite senses of the twist angle of the LC directors in the bulk. Detailed analysis of the type 1 exposure geometry will be published elsewhere. The exposure of the PIA-1 film was carried out using one linearly *p*-polarized beam from a He-Cd laser ($\lambda=325$ nm) through a photomask, incident on the sample from the PIA-1 film side with an intensity of 6 mW/cm^2 at oblique incidence (20° to the surface normal). The exposure time was set to 3 h. After exposure to the polarized laser light, the masked areas prevented uv illumination of the underlying substrate and thus preserved the original homeotropic alignment property of PIA-1. However, PIA-1 undergoes photo-dissociation [21,22] and planar alignment of the LC molecules occurs in the uv-exposed regions. By performing separate preliminary experiments, it was observed that the alignment direction of the LC produced in the uv-exposed PIA-1-coated substrate surface was parallel to the polarization direction of the linearly *p*-polarized laser light. Moreover, the pretilt angle of a nematic LC in contact with the uv-exposed PIA-1-coated substrate surface was found to be 0.12° by the ellipsometric measurement method using cells with antiparallel alignment [17]. Hence, the alignment patterns were alternating planar (exposed) and homeotropic (masked) stripes. Even though the micropatterned surface provides two equilibrium states with equal energy minimum, the formation of two domains with equal probability of occurring will depend on the LC materials, cell configurations and other physical parameters such as polar and azimuthal anchoring strengths. Five cell configurations are possible with regard to a micropatterned surface. The micropatterned surface can be used opposite either a homeotropic or planar surface. In configuration 1, a micropatterned surface was placed opposite a homeotropic surface. This gives two hybrid aligned nematic (HAN) states [17]. In configuration 2, a micropatterned surface was placed opposite a planar surface in which the polarization direction of the linearly polarized laser light was set to be parallel to the rubbing direction. This arrangement induces a homogeneous state and a splay state. Here, it should be noted that the alignment direction of the LC produced in the uv-exposed PIA-1-coated substrate surface was parallel to the polarization direction of the linearly *p*-polarized laser light. In configuration 3, a micropatterned surface was placed opposite a planar surface in which the polarization direction of the linearly polarized laser light was set to be perpendicular to the rubbing direction. This gives two oppositely twisted states

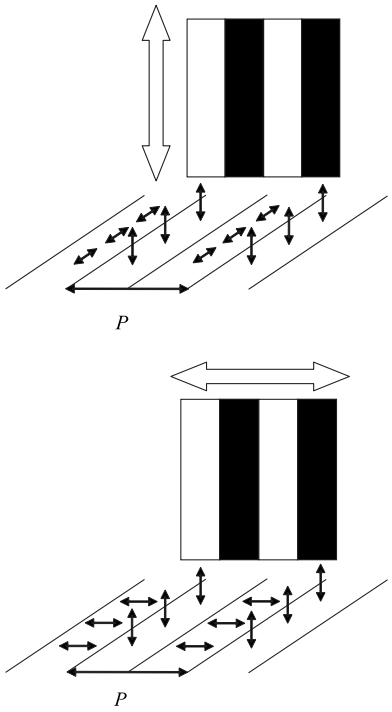

FIG. 1. Two types of geometries of the linearly polarized laser exposure and schematic illustration of the textured stripe patterns with alternating planar and homeotropic anchorings. The dark arrows indicate LC directors and the white arrows represent the direction of the polarization of linearly polarized laser light. *P* denotes the stripe pattern periodicity. (a) Type 1 exposure geometry; (b) type 2 exposure geometry.

[19]. In configurations 4 and 5, the two micropatterned surfaces were placed opposite one another in which the polarization directions of the linearly polarized laser light on the two substrate surfaces were set to be parallel or anti-parallel. This gives a splay state or a homogeneous state, respectively provided that only one domain is formed on the micropatterned surface and the azimuthal anchoring energy on the planar stripes is greater than the critical azimuthal anchoring energy as recently reported by Atherton and Sambles [23]. The latter condition is only concerned with the formation of the splay state.

D. Preparation of LC cells for memory imprinting

LC cells were prepared with one plate coated with bare untreated ITO film and a counter-plate fabricated with a micropatterned PIA-1-coated substrate. The cells were filled with 5CB by capillary action in the isotropic phase. We then gradually cooled the sample cell to room temperature while maintaining a thermal gradient between the plate and the counterplate. The temperature of the plate coated with bare untreated ITO film was relatively higher than that of the counter-plate fabricated with a micropatterned PIA-1-coated substrate. The properties of 5CB were the same as mentioned above.

E. STM and AFM measurements

STM (Unisoku, Japan) and AFM (SPM-9500J2, Shimadzu) were used to perform surface characterization of the ITO samples. The root-mean-square (rms) values used in this paper for surface roughness were calculated using the off-line analysis software of the SPM-9500J2, and these values signify the rms average between the height deviations and the mean line or surface, taken over the evaluation length or area.

III. RESULTS AND DISCUSSION

A. STM and AFM observations

The surfaces of the ITO samples were examined by STM and AFM operating in a dynamic mode. Figures 2(a) and 2(b) show STM images of the two types of ITO films (ITO-NS and ITO-CN). The granular structure of the ITO surface can be clearly seen in both types of films, with the grains having dimensions on the order of nm. However, the two types have different structural arrangements and shapes. These STM observations were reinforced by AFM analysis. Figure 3(a) shows a three-dimensional view of the AFM data of ITO-NS and Fig. 3(b) shows a two-dimensional view of the AFM data of ITO-NS indicating rms line roughness and size of a pillar-shaped grain. Moreover, Fig. 3(c) reveals a two-dimensional view of the data shown in Fig. 3(b) showing the rms area roughness. Similarly, Fig. 4(a) shows a three-dimensional view of the AFM data of ITO-CN and Fig. 4(b) shows a two-dimensional view of the AFM data of ITO-CN indicating rms line roughness and the size of a domain. Figure 4(c) reveals a two-dimensional view of the data shown in Fig. 4(b) showing the rms area roughness. It was found that both the rms line and area roughness of ITO-NS

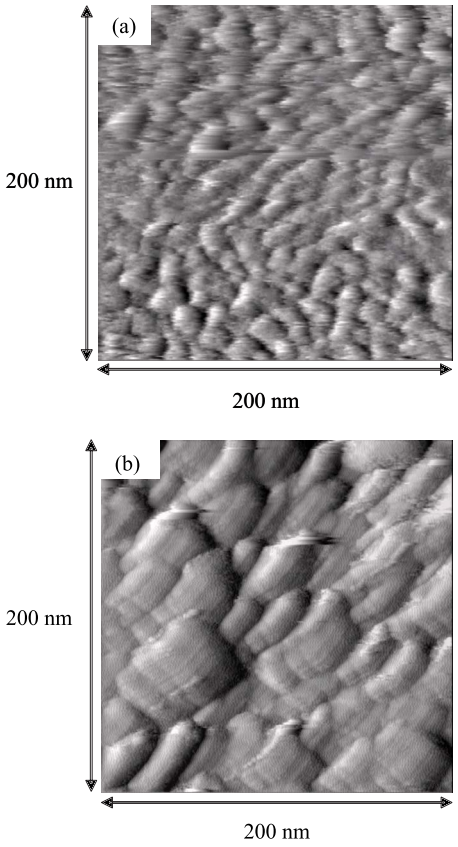

FIG. 2. STM images of the (a) ITO-NS surface and (b) ITO-CN surface. Scan size is 200×200 nm^2.

were less than those of ITO-CN. Moreover, the granular structure of the ITO-NS film cannot be clearly seen and some pillar-shaped grains were observed prominently. In contrast to the ITO-NS film, individual grains of the ITO-CN film can be seen clearly and grains were embedded in the domain structures. Such differences will depend on a number of parameters such as the deposition techniques, physical treatment (polishing procedure and polishing times), and thickness of the ITO films [24–26].

B. Alignment of LC on bare untreated ITO

To examine the orientational behavior of LCs on bare untreated ITO surfaces, LC cells were fabricated with two pieces of bare untreated ITO-coated substrates. The cells were filled with 5CB by capillary action in the isotropic phase and gradually cooled down to room temperature. Figure 5 shows polarized microphotographs of an LC cell fabricated with two bare untreated ITO-NS-coated substrates between crossed polarizers. The so-called continuously degenerate azimuthal anchoring [27,28] with the Schlieren texture of 5CB was observed. However, a homeotropic orientation of 5CB was achieved in an LC cell sandwiched between two bare untreated ITO-CN-coated substrates as shown in Fig. 6. Therefore, these results suggest that the structural morphology of the ITO substrate and the interfacial origin of the LC anchorage [29–31] play a defining role in determin-

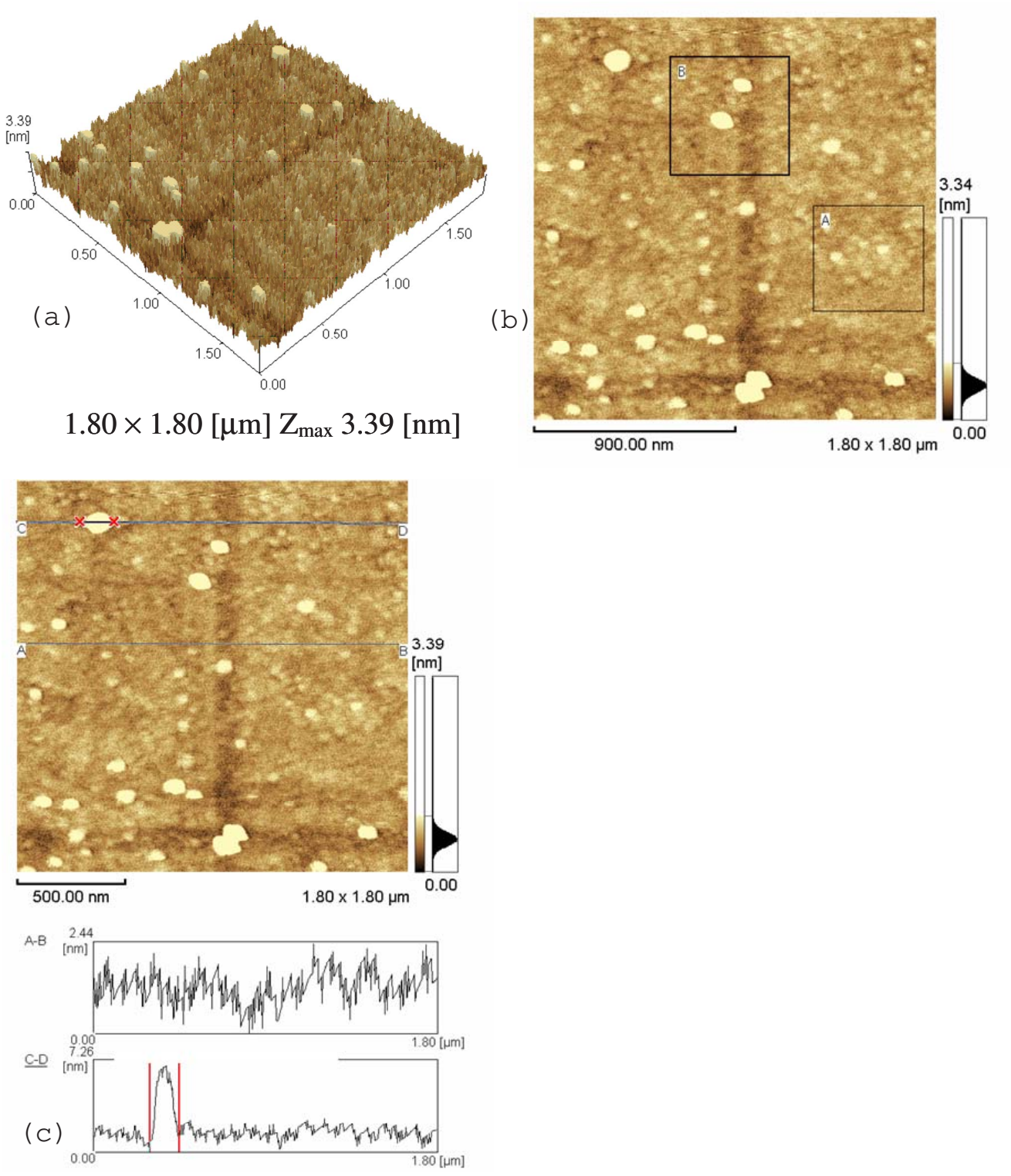

FIG. 3. (Color online) $1.8 \times 1.8\ \mu m^2$ dynamic mode AFM image of the ITO-NS surface. (a) Three-dimensional view of the AFM data. (b) Two-dimensional view of the AFM data showing rms line roughness: (i) rms line roughness of line $AB=0.43$ nm, (ii) rms line roughness of line $CD=1.11$ nm, and (iii) size of a pillar-shaped grain $=0.16\ \mu m$. (c) Two-dimensional view of the same data showing rms area roughness: (i) rms area roughness of region $A=0.425$ nm and (ii) rms area roughness of region $B=0.824$ nm.

ing the alignment of a LC whether it is planar [4,32] or homeotropic [26,33–35]. It was also observed that the continuously degenerate azimuthal alignment on bare untreated ITO-NS-coated substrates remains unchanged; however, the homeotropic alignment on the bare untreated ITO-CN-coated substrates undergoes transition to planar alignment over time, as shown in Fig. 7. Here, we assume that the destabilizing surface polarization mechanism may lead to the de-

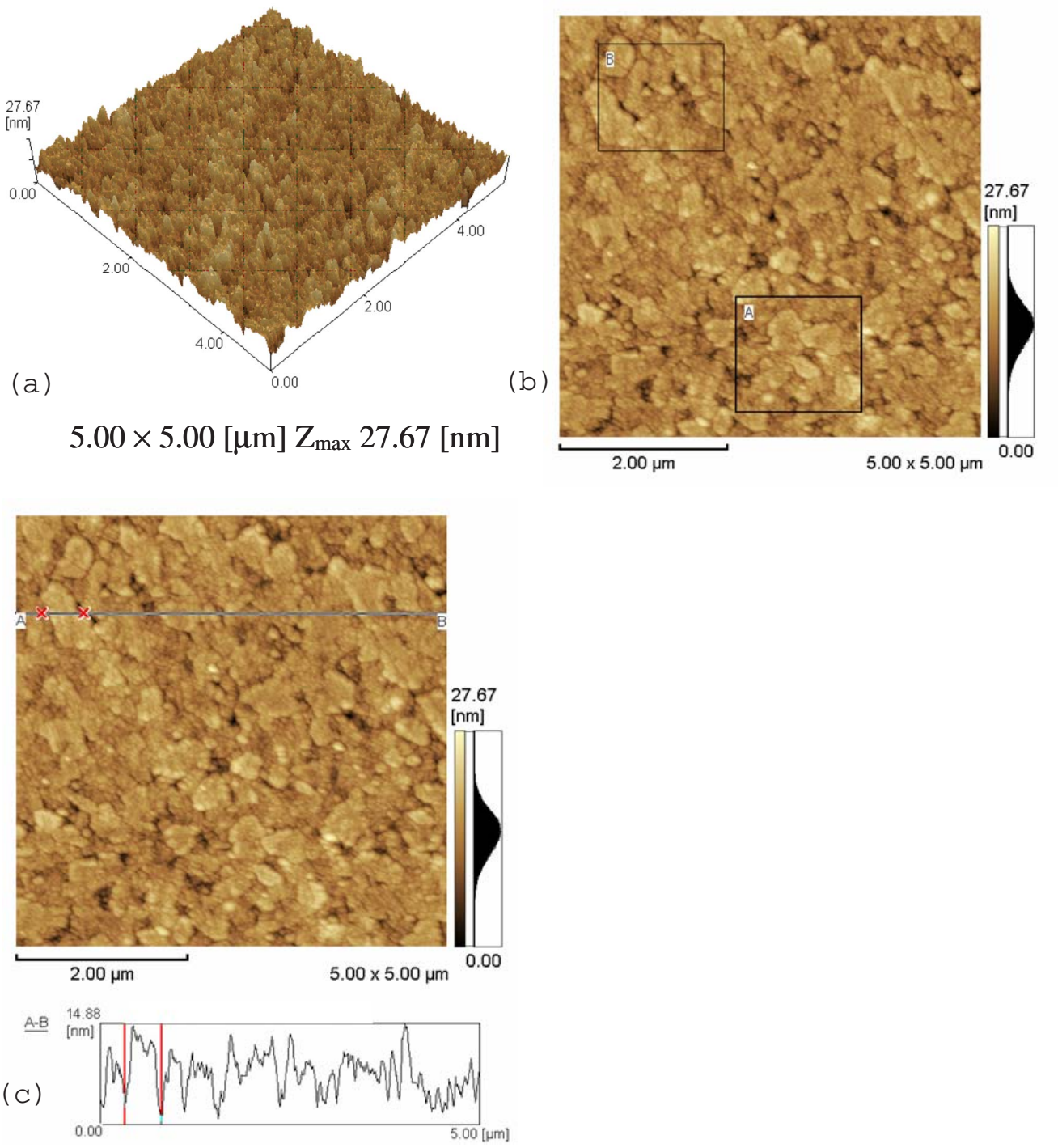

FIG. 4. (Color online) 5×5 μm^2 dynamic mode AFM image of the ITO-CN surface. (a) Three-dimensional view of the AFM data. (b) Two-dimensional view of the AFM data showing rms line roughness: (i) rms line roughness of line $AB=2.93$ nm and (ii) size of a domain$=0.49$ μm. (c) Two-dimensional view of the same data showing rms area roughness: (i) rms area roughness of region $A=3.515$ nm and (ii) rms area roughness of region $B=3.005$ nm.

struction of the homeotropic alignment of a polar liquid crystal (5CB) at the ITO-CN-coated substrate surface [36]. This unexpected and interesting observation needs additional study to be explored in detail and is outside the scope of this paper. For the purpose of our study, bare untreated ITO-NS-coated substrates were used for the memory imprinting process since they show no alignment degradation over time.

C. Measurement of pretilt angle, polar anchoring strength and azimuthal anchoring strength of a homogeneously aligned nematic LC cell using micropatterned substrates

Antiparallel homogeneous cells were prepared using micropatterned substrates. Nematic LC used was 5CB (Merck, Japan). The pretilt angle and polar anchoring strength were measured by symmetrically oblique incidence transmission

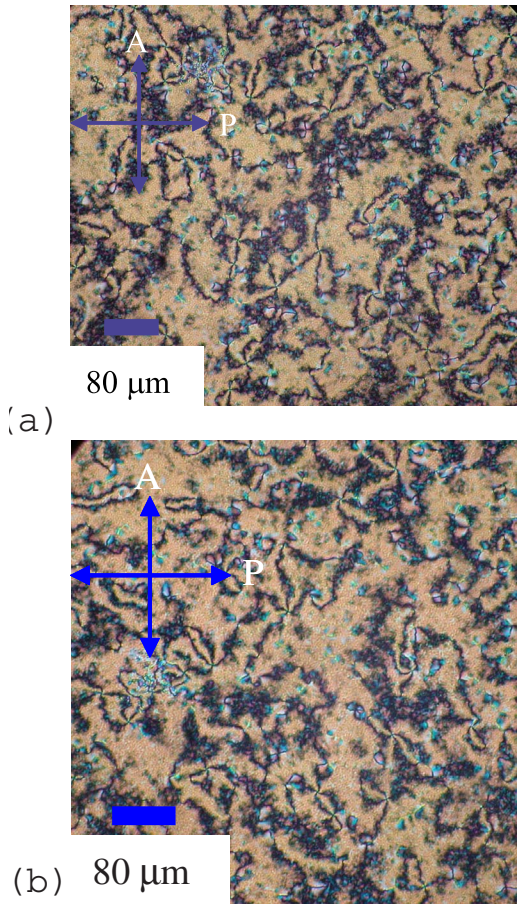

FIG. 5. (Color online) Polarized microphotographs of an LC cell (LC: 5CB; nominal cell gap=5.12 μm) fabricated with two bare untreated ITO-NS-coated substrates. The images indicate (a) 0° and (b) 45° rotation of the sample between crossed polarizers.

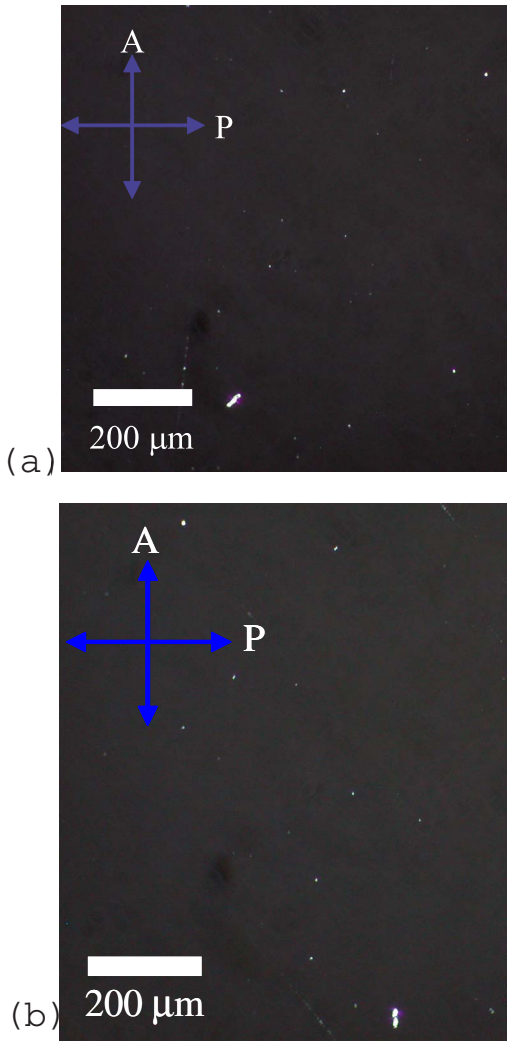

FIG. 6. (Color online) Polarized microphotographs of an LC cell (LC: 5CB; nominal cell gap=3.59 μm) fabricated with two bare untreated ITO-CN-coated substrates, at (a) 0° and (b) 45° rotation of the sample between crossed polarizers.

ellipsometry (SOITE) [37–39]. By using SOITE method, the polar anchoring strength can be determined accurately without the effect of multiple-beam interference (MBI). As we know, the ellipsometric parameter Δ, which represents the phase difference between *p*-polarized and *s*-polarized light, is measured to obtain the optical properties of the sample. When the refractive index of a thin film is different from that of the exterior refractive index, multiple-beam reflection, and MBI occur. Therefore, phase difference Δ between *p*-polarized and *s*-polarized light transmitted through a LC cell is by no means equal to retardation R of a LC layer. As a result, Δ involves not only the retardation R of the layer but also the MBI. If the phase differences between *p*-polarized and *s*-polarized light for $+\beta$ and $-\beta$ incidence angles are denoted as Δ^+ and Δ^-, respectively, it has been shown theoretically that $\Delta^- - \Delta^+ = R(-\beta) - R(+\beta)$ where $R(+\beta)$ and $R(-\beta)$ represent genuine retardations of a LC for $+\beta$ and $-\beta$ incidence angles, provided that the director is in the incidence plane of light beam. The applied voltage dependence of $\Delta^- - \Delta^+$ of a homogeneously aligned nematic cell having LC with a positive dielectric anisotropy is a function of $V_c = \pi(K_{11}/\varepsilon_0 \Delta\varepsilon)^{1/2}$, $\kappa = (K_{33} - K_{11})/K_{11}$, $\gamma = (\varepsilon_\parallel - \varepsilon_\perp)/\varepsilon_\perp$, cell gap d, pretilt angle θ_p, and the normalized polar anchoring strength $A = W_\theta d/K_{11}$ provided that refractive indices n_e and n_o are given. In our experiments, Δ was measured using the polarization modulated spectroscopic ellipsometer (PMSE) (M-150, JASCO) equipped with a photoelastic modulator. By fitting the experimental result with the theoretical one, we can obtain the above-mentioned six parameters simultaneously by polytope method. Figure 8 shows the experimental and theoretical results of dependence of $\Delta^- - \Delta^+$ on applied voltage. The experimental result was fitted with $\theta_p = 50°$, $W_\theta = 5.0 \times 10^{-4}$ J m^{-2}, $d = 9.97$ μm, $\beta = 45°$, and $\lambda = 500$ nm. Moreover, the azimuthal anchoring strength was estimated by measuring the widths of the surface disclination lines of Néel type as proposed by Kléman and Williams [40]. Porte used this method to estimate the azimuthal anchoring energy for highly tilted surfaces [41]. Kléman and Williams determined a relationship between the width of surface disclination of Néel type, w and the azimuthal anchoring energy, W_ϕ resulting in $W_\phi \sim (\pi^2 d/4w^2)(K_{11} + K_{33})$ where d is a cell gap and K_{11} and K_{33} are the elastic constants for splay and bend deformations, respectively. We estimated that 3.74×10^{-6} J m$^{-2} < W_\phi < 4.33 \times 10^{-5}$ J m^{-2} with d

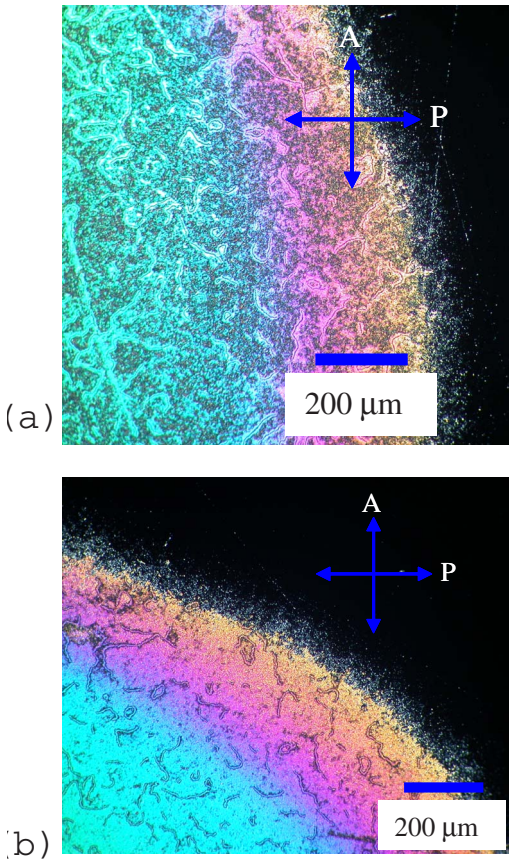

FIG. 7. (Color online) Polarized microphotographs of an LC cell (LC: 5CB; nominal cell gap=3.59 μm) fabricated with two bare untreated ITO-CN-coated substrates, showing homeotropic-to-planar transition over time, at (a) 0° and (b) 45° rotation of the sample between crossed polarizers.

=9.97 μm, 3.1 μm$<w<$10.55 μm, splay and bend elastic constants of 5CB: K_{11}=7.1 pN and K_{33}=9.8 pN.

D. Memory imprinting

Thin LC cells were prepared with one plate coated with the bare untreated ITO-NS film and a counterplate fabricated

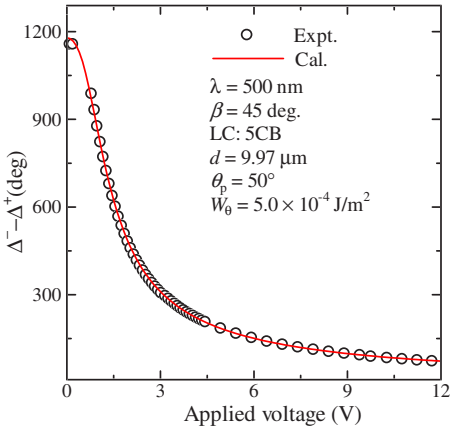

FIG. 8. (Color online) Experimental and theoretical results of dependence of $\Delta^- - \Delta^+$ on applied voltage for a homogeneously aligned nematic LC cell using micropatterned substrates.

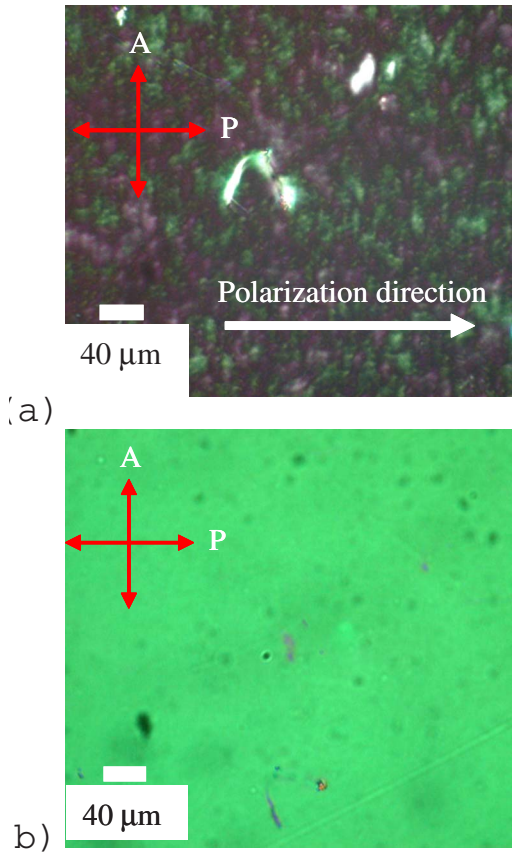

FIG. 9. (Color online) Polarized microphotographs of a memory-induced LC cell (LC: 5CB; nominal cell gap=3.4 μm) at (a) 0° and (b) 45° rotation of the sample between crossed polarizers.

with a micropatterned PIA-1-coated substrate. 5CB was introduced into the cell in the isotropic phase to prevent flow complications. The sample was cooled to the nematic phase with the micropatterned substrate at a lower temperature than the bare untreated ITO substrate. The nematic state appears first, close to the micropatterned substrate, and propagates its order through the bulk to the bare untreated ITO substrate. When the nematic phase encounters the initially isotropic untreated ITO substrate, the micropatterned orientation is imprinted on the ITO and is memorized on the surface by the adsorption of an oriented nematic layer. The adsorbed layer behaves as a new anisotropic substrate imposing strong, inhomogeneous, monostable anchoring since it is due to the local configuration of the LC material at first contact with the surface [8,28,42–45]. Figure 9 shows polarized microphotographs of a memory-induced LC cell between crossed polarizers. Since the micropatterned surface provides two equilibrium states with equal energy minima, we expected that these two equilibrium states will be imprinted on the bare untreated ITO substrate. However, when we carefully examined the textures of a memory-induced LC cell (Fig. 9), the polarizing optical microscopy reveals that there are two states, viz. a homogeneously tilted state (fairly dark) and a π-twisted state (pale green) instead of two oppositely tilted states. Here, the formation of π-twisted state was confirmed due to light transmission at both conditions (i) between crossed polarizers [Fig. 9(a)] and (ii) at 45° rotation of the

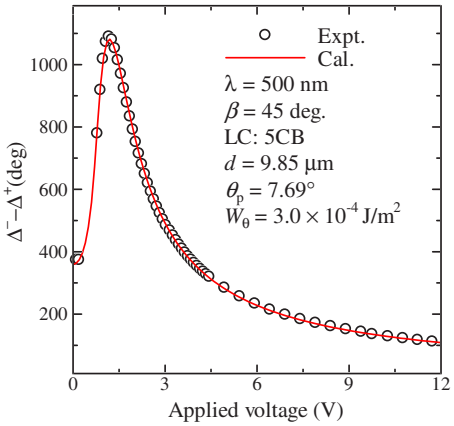

FIG. 10. (Color online) Experimental and theoretical results of dependence of $\Delta^- - \Delta^+$ on applied voltage for a homogeneously aligned nematic LC cell using imprinted ITO substrates.

sample between crossed polarizers [Fig. 9(b)] when the transmission axis of the polarizer was parallel to the polarization direction of the linearly polarized laser light on the micropatterned substrate surface. Moreover, we considered that one of the equilibrium states was imprinted on the bare untreated ITO substrate because the adsorbed layer on ITO substrate exhibits a monostable anchoring. Therefore, it is assumed that the bistable nature of the micropatterned surface was mediated by the formation of a π-twisted state. Besides, these two states are stable to the nematic-isotropic phase transition, indicating the presence of a firmly adsorbed layer of LC molecules. The memory-induced LC alignment remains stable without any degradation over time.

E. Measurement of pretilt angle, polar anchoring strength and azimuthal anchoring strength of a homogeneously aligned nematic LC cell using imprinted ITO substrates

To show that the memory imprinting indeed had occurred on the bare untreated ITO surface, two LC cells were prepared with one plate coated with the bare untreated ITO-NS film, and a counterplate fabricated with a micropatterned

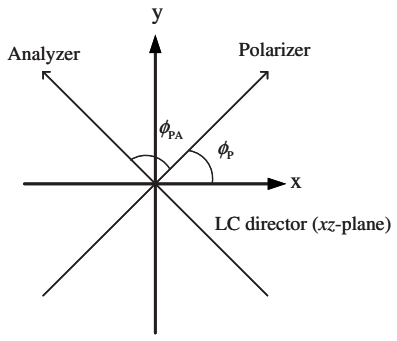

FIG. 11. Direction of polarizers and LC cell relative to the x axis and each other. Let the xy plane be the LC cell substrate surfaces, and the xz plane be the plane containing LC directors. ϕ_P is the angle between the x axis and the polarizer, and ϕ_{PA} is the angle between the polarizer and the analyzer.

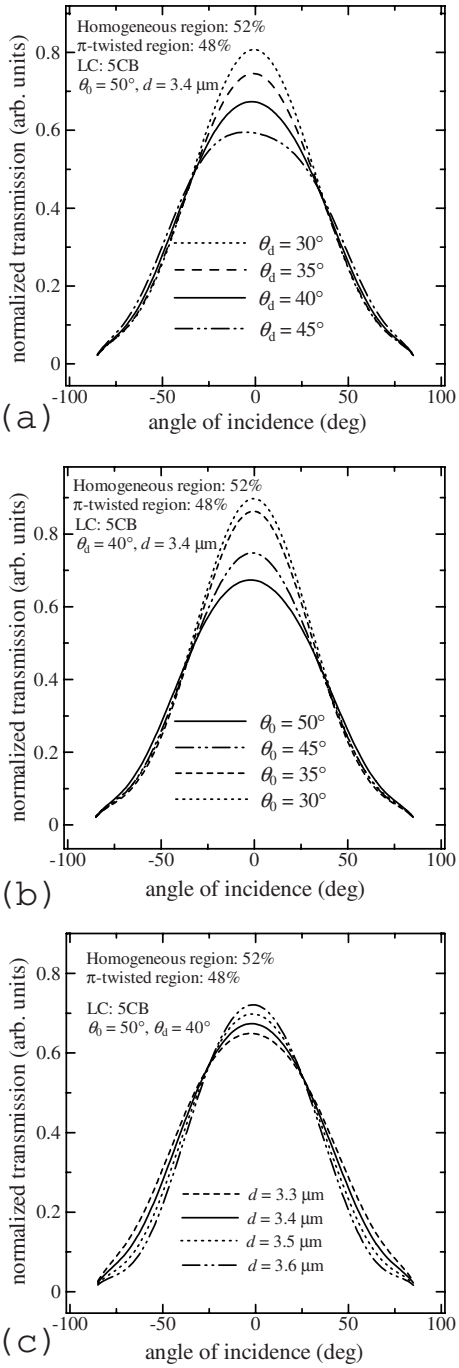

FIG. 12. Examples of theoretical curves for the relationship between normalized transmission and incident angle for a sample LC cell: (a) Varying different pretilt angles on the memory-aligned ITO substrate surface, (b) varying different pretilt angles on the micropatterned substrate surface, and (b) varying different cell thicknesses.

PIA-1-coated substrate by performing the same procedures mentioned in Sec. III D except that the two substrates were gripped by clips instead of sealing them with epoxy. Then, the imprinted ITO substrate was separated from the micropatterned PIA-1-coated substrate, and LC molecules on the imprinted ITO substrate were washed with toluene (Nacalai Tesque, Inc., Japan). It is supposed that almost all the LC

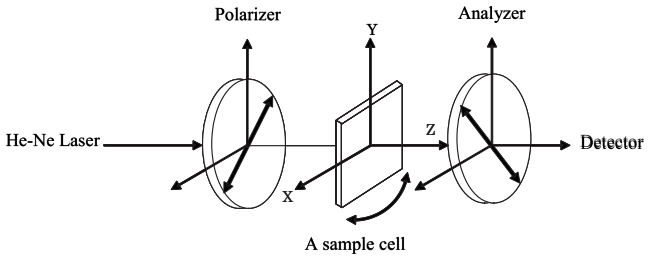

FIG. 13. Optical setup used to determine the relationship between normalized transmission and incident angle for a memory-induced LC cell.

molecules were removed except LC molecules locating at the vicinity of the imprinted ITO substrate as reported in [46]. Finally, we piled the two imprinted ITO substrates one on top of the other to form an antiparallel homogeneous cell, and 5CB (Merck, Japan) was introduced into the cell in the isotropic phase. The pretilt angle and polar anchoring strength were measured by SOITE method. Figure 10 shows the experimental and theoretical results of dependence of $\Delta^- - \Delta^+$ on applied voltage. The experimental result was fitted with $\theta_p = 7.69°$, $W_\theta = 3.0 \times 10^{-4}$ J m^{-2}, $d = 9.85$ μm, $\beta = 45°$, and $\lambda = 500$ nm. Moreover, the azimuthal anchoring strength was estimated by measuring the widths of the surface disclination lines of Néel type mentioned in Sec. III C. We estimated that 2.24×10^{-5} J m$^{-2} < W_\phi < 1.3 \times 10^{-4}$ J m^{-2} with $d = 9.85$ μm, 2 μm $< w <$ 4.28 μm, splay and bend elastic constants of 5CB: $K_{11} = 7.1$ pN and $K_{33} = 9.8$ pN. From these results, it was confirmed that we succeeded in imprinting a high tilt on the ITO substrate, and the imprinted tilt angle on ITO substrate was lower than that on the counter-micropatterned substrate. This difference in pretilt angle is presumably related to the surface energies of the respective substrate surfaces as reported by Toko *et al.* [47]. Moreover, it is noteworthy that the azimuthal anchoring strength on the imprinted ITO substrate was one order of magnitude greater than that on the micropatterned PIA-1-coated substrate.

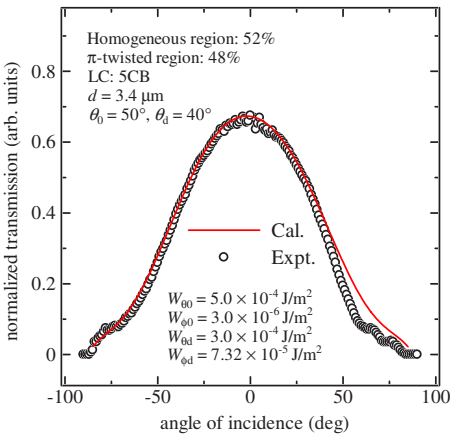

FIG. 14. (Color online) Relationship between normalized transmission and incident angle for a memory-induced LC cell, showing an experimental result together with a calculated value.

F. Evaluation of a pretilt angle on the memory-aligned ITO substrate using a memory-induced LC cell

The idea of determining pretilt angles at the surfaces of substrates in the three types (homeotropic, homogeneous, and twisted) of LC cells from angular-dependent optical transmission was firstly proposed by Baur *et al.* [48]. Nakano *et al.* and Scheffer *et al.* reported modified and different approaches to Baur's crystal rotation method [49,50]. Dyadyusha *et al.* recently used Baur's method to measure the pretilt angle of an oblique orientation of nematic LC on a polyvinylcinnamate surface [51]. In this study, we have developed an angular-dependent optical transmission method to determine a pretilt angle on the memory-aligned ITO substrate using the memory-induced LC cell having a homogeneously tilted state and a π-twisted state. The angular-dependent optical transmission method has its advantages and limitation. Using this method, we can measure a sample cell in which one of the substrate surfaces exhibits two different states having oppositely tilted or twisted configurations or a combination of other configurations provided that the pretilt angle of a countersubstrate will be known (90° in the case of a homeotropic alignment) or must be predetermined.

Theoretical derivations for the angular-dependent optical transmission method were carried out as follows. The incident light is described by the Jones vector:

$$\begin{bmatrix} E_{\mathrm{ip}} \\ E_{\mathrm{is}} \end{bmatrix} = \begin{bmatrix} \cos \phi_P \\ \sin \phi_P \end{bmatrix}, \tag{1}$$

where E_{ip} and E_{is} represent the complex amplitudes of the components of the electric vectors of the incident waves, and ϕ_P is the angle between the x axis and the polarizer as illustrated in Fig. 11.

The transmitted light is described by

$$\begin{bmatrix} E_{\mathrm{tp}} \\ E_{\mathrm{ts}} \end{bmatrix} = \begin{bmatrix} t_p^{\mathrm{ga}} & 0 \\ 0 & t_s^{\mathrm{ga}} \end{bmatrix} \begin{bmatrix} \tau_{\mathrm{pp}} & \tau_{\mathrm{ps}} \\ \tau_{\mathrm{sp}} & \tau_{\mathrm{ss}} \end{bmatrix} \begin{bmatrix} t_p^{\mathrm{ag}} & 0 \\ 0 & t_s^{\mathrm{ag}} \end{bmatrix} \begin{bmatrix} E_{\mathrm{ip}} \\ E_{\mathrm{is}} \end{bmatrix}, \tag{2}$$

where E_{tp} and E_{ts} represent the complex amplitudes of the components of the electric vectors of the transmitted waves. The terms t_p^{ag}, t_s^{ag}, t_p^{ga}, and t_s^{ga} are Fresnel's transmission coefficients for p- and s-polarized lights at the air-glass and glass-air interfaces, respectively. τ_{pp}, τ_{ps}, τ_{sp}, and τ_{ss} denote the transmission Jones coefficients of the LC layer with ITO and alignment films, which were calculated by the Berreman 4×4 matrix method [52]. It is noteworthy that the 4×4 matrix method is not applicable to the glass substrate used in our experiments, since the glass substrate used is sufficiently thick compared to the wavelength of the incident light, and the nonuniformity of the thickness over the glass substrate is also larger than the wavelength. Therefore, the optical transmission at the glass substrate was estimated using Fresnel's formula.

The total intensity of the transmission is given by

$$T = |E_{\mathrm{tp}} \cos \phi_A + E_{\mathrm{ts}} \sin \phi_A|^2, \tag{3}$$

where $\phi_A = \phi_P + \phi_{\mathrm{PA}}$.

Figure 12 shows some examples of theoretical curves for the relation between the normalized transmission and the incident angle for a sample LC cell. The main fitting param-

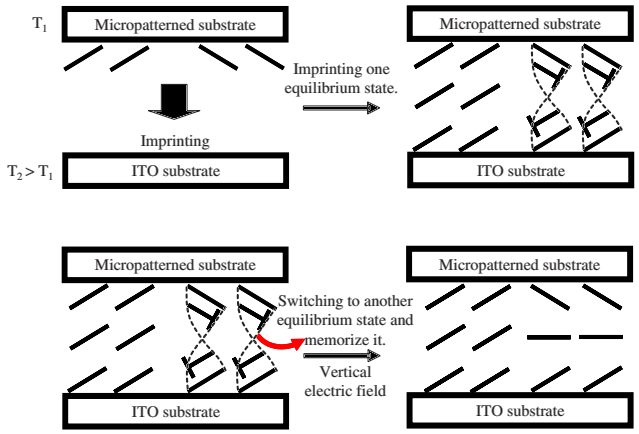

FIG. 15. (Color online) Schematic diagrams of the memory imprinting process and switching behavior of a memory-induced LC cell.

eters are θ_0, θ_d, and d, where θ_0 and θ_d denote pretilt angles at $z=0$ (micropatterned substrate surface) and $z=d$ (memory-aligned ITO substrate surface), and d represents a cell thickness. Polar and azimuthal anchoring energies at both substrates will be taken into account in the fitting parameters. The value of pretilt angle on the micropatterned substrate surface obtained by SOITE method will be used as a reference. Therefore, the pretilt angle on the memory-aligned ITO substrate surface, cell thickness, polar and azimuthal anchoring energies at both substrates, the occupation ratio of two different regions can be determined by fitting the theoretical values to the experimental data obtained by the measurement of the normalized transmission and the incident angle.

Figure 13 depicts an optical setup used to determine the relationships between the normalized transmission and the incident angle for a memory-induced LC cell. A sample LC cell was adjusted between crossed polarizers so that the LC director makes an angle of 45° with respect to both their axes. The sample cell was rotated around the OY axis, perpendicular to the director. The dependence of the normalized transmission on the incident angle between the He-Ne laser beam ($\lambda=632.8$ nm) and the cell normal was measured. Figure 14 shows the experimental results together with the calculated values for the relationship between the normalized transmission and the incident angle for a memory-induced LC cell. The experimental result was fitted with $\theta_0=50°$, $\theta_d=40°$, $d=3.4$ μm, $W_{\theta 0}=5.0\times10^{-4}$ J m^{-2}, $W_{\phi 0}=3.0\times10^{-6}$ J m^{-2}, $W_{\theta d}=3.0\times10^{-4}$ J m^{-2}, and $W_{\phi d}=7.32\times10^{-5}$ J m^{-2}. It was found that 52% of the memory-induced LC cell is a homogeneous region and other 48% of the cell is a π-twisted region. Moreover, it was also observed that the pretilt angle on the memory-aligned ITO substrate was greater than that on the imprinted ITO substrate due to the property of bulk effect.

G. Switching behavior of a memory-induced LC cell

Figure 15 depicts schematic diagrams of the memory imprinting process and the switching behavior of a memory-induced LC cell. It was previously mentioned that two states,

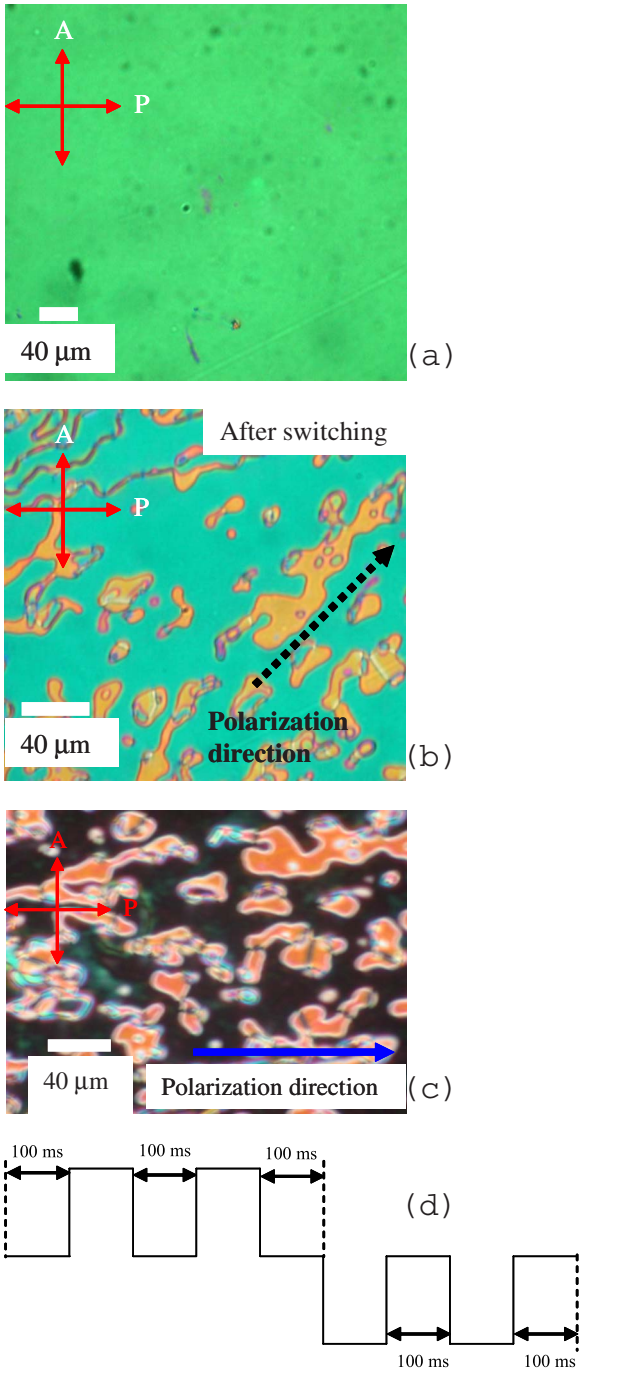

FIG. 16. (Color online) Polarized microphotographs of a memory-induced LC cell (LC: 5CB; nominal cell gap=3.4 μm): (a) No applied voltage, (b) and (c) switching to another equilibrium state. Here, the polarized microphotographs were taken at (b) 45° and (c) 0° rotation of the sample between crossed polarizers. (d) Scheme of applied voltage pulses with pulse widths=100 ms and pulse amplitude=20 V.

namely a homogeneously tilted state and a π-twisted state were formed during memory imprinting process. By means of a vertical field effect, microscopic switching of a π-twisted state to another equilibrium state was observed and this new equilibrium state was found to be memorized after the applied electric field was turned off. Images of

switching in a memory-induced LC cell are shown in Fig. 16. The switching mechanism is outlined as follows. The micropatterned surface provides two equilibrium states with equal energy minima. In the memory imprinting process, one equilibrium state was imprinted on the bare untreated ITO substrate but another equilibrium state was masked. Instead, a π-twisted state was formed. Under the influence of a vertical electric field, the π-twisted state switches to a splay state via the propagation of the disclinations with the help of the bistable nature of the micropatterned surface. It appears that the intrinsically existing second equilibrium state, which was masked, is revealed with the assistance of a vertical electric field. Since the two configurations, i.e., a π-twisted state and a splay state are topologically distinct from each other, a transition between the two configurations is necessarily accompanied by a discontinuous change in alignment as predicted by Porte [53]. That is, switching between these states occurs in an electric field, which involves the motion of the disclination. During switching, the process of domain formation, domain growth and motion of the disclination lines were actually observed. Immediately after switching off, we observed a relaxation process in a new equilibrium state. After the relaxation, multifarious LC textures consisting of a homogeneously tilted state (dark), a splay state (bright brownish texture), and other textures similar to nematic marbled textures were observed, as shown in Fig. 16(c), and the new state was found to be memorized. The new memory state is stable to the nematic-isotropic phase transition, indicating the presence of a firmly adsorbed layer of LC molecules. This can be erased by heating to temperatures considerably above the nematic-isotropic phase transition. However, after limited thermal cycling, the new memory state cannot be erased up to the isotropic state.

IV. CONCLUSIONS

We investigated memory alignment of nematic LCs on isotropic bare untreated ITO substrates by imprinting a micropatterned orientation on the ITO substrates. It was confirmed that we succeeded in imprinting a high tilt on the ITO substrate and the imprinted pretilt angle on the ITO substrate was lower than that on the counter-micropatterned substrate. It was found that one of two equilibrium states provided by the micropatterned surface was imprinted on the bare untreated ITO substrate but another equilibrium state was masked in the memory imprinting process. It was observed that the second equilibrium state, which was masked, is revealed with the assistance of a vertical electric field. A dynamical model may be needed to help us fully understand the switching process. Further experiments are currently in progress.

ACKNOWLEDGMENTS

We would like to express our sincere thanks to Professor K. Yasui, Department of Electrical Engineering, Nagaoka University of Technology, for providing STM facilities. This work was partially supported by the 21st century COE program "Creation of Hybridized Materials with Super-Functions and Formation of International Research and Education Centre" from the Ministry of Education, Culture, Sports, Science and Technology, Japan.

[1] G. Friedel, Ann. Phys. (Paris) **18**, 273 (1922).
[2] N. A. Clark, Phys. Rev. Lett. **55**, 292 (1985).
[3] Y. Ouchi, M. B. Feller, T. Moses, and Y. R. Shen, Phys. Rev. Lett. **68**, 3040 (1992).
[4] H. Dreyfus-Lambez, D. Stoenescu, I. Dozov, and Ph. Martinot-Lagarde, Mol. Cryst. Liq. Cryst. Sci. Technol., Sect. A **352**, 453 (2000).
[5] L. V. Tsonev, M. P. Petrov, and G. Barbero, Liq. Cryst. **24**, 853 (1998).
[6] M. Petrov and L. Tsonev, Liq. Cryst. **29**, 743 (2002).
[7] S. Sato and M. Wada, Jpn. J. Appl. Phys. **11**, 1566 (1972).
[8] J. Cheng and G. D. Boyd, Appl. Phys. Lett. **35**, 444 (1979).
[9] N. Koshida and S. Kikui, Appl. Phys. Lett. **40**, 541 (1982).
[10] T. Nose, S. Masuda, and S. Sato, Jpn. J. Appl. Phys., Part 1 **30**, 3450 (1991).
[11] R. Yamaguchi and S. Sato, Jpn. J. Appl. Phys., Part 2 **30**, L616 (1991).
[12] P. Vetter, Y. Ohmura, and T. Uchida, Jpn. J. Appl. Phys., Part 2 **32**, L1239 (1993).
[13] M. Kawasumi, N. Hasegawa, A. Usuki, and A. Okada, Liq. Cryst. **23**, 769 (1996).
[14] R. Kravchuk and O. Yaroshchuk, Mol. Cryst. Liq. Cryst. **422**, 385 (2004).
[15] G. D. Boyd, J. Cheng, and P. D. T. Ngo, Appl. Phys. Lett. **36**, 556 (1980).
[16] I. Dozov and G. Durand, Liq. Cryst. Today **8**, 1 (1998).
[17] T. N. Oo, R. Bansho, N. Tanaka, M. Kimura, and T. Akahane, Jpn. J. Appl. Phys., Part 1 **45**, 4176 (2006).
[18] T. N. Oo, M. Kimura, and T. Akahane, in *Proceedings of the 13th International Display Workshops (IDW '06), Otsu, Japan, 2006*, p. 99.
[19] T. N. Oo, Y. Yasu, M. Kimura, and T. Akahane, in *Abstracts of the Japanese Liquid Crystal Society Annual Meetings, Akita University, Japan, 2006*, p. 287.
[20] M. O'Neill and S. M. Kelly, J. Phys. D **33**, R67 (2000).
[21] M. Hasegawa and Y. Taira, J. Photopolym. Sci. Technol. **8**, 241 (1995).
[22] Y. Iimura and S. Kobayashi, SID Int. Symp. Digest Tech. Papers **28**, 311 (1997).
[23] T. J. Atherton and J. R. Sambles, Phys. Rev. E **74**, 022701 (2006).
[24] T. Asikainen, M. Ritala, M. Leskelä, T. Prohaska, G. Friedbacher, and M. Grasserbauer, Appl. Surf. Sci. **99**, 91 (1996).
[25] J. Hoogboom, M. Behdani, J. A. A. W. Elemans, M. A. C. Devillers, R. de Gelder, A. E. Rowan, Th. Rasing, and R. J. M. Nolte, Angew. Chem., Int. Ed. **42**, 1812 (2003).
[26] J. G. Fonseca, Ph.D. thesis, Université Louis Pasteur, Strasbourg, 2001.

[27] P. G. de Gennes and J. Prost, *The Physics of Liquid Crystals*, 2nd ed. (Clarendon Press, Oxford, 1993), p. 163.
[28] I. Dozov, D. N. Stoenescu, S. Lamarque-Forget, Ph. Martinot-Lagarde, and E. Polossat, Appl. Phys. Lett. **77**, 4124 (2000).
[29] J. E. Proust, L. Ter-Minassian-Saraga, and E. Guyon, Solid State Commun. **11**, 1227 (1972).
[30] E. Perez, J. E. Proust, and L. Ter-Minassian-Saraga, Mol. Cryst. Liq. Cryst. **42**, 167 (1977).
[31] B. Jérôme, Rep. Prog. Phys. **54**, 391 (1991).
[32] I. Dierking, J. Phys. D **34**, 806 (2001).
[33] O. D. Lavrentovich, V. G. Nazarenko, V. V. Sergan, and G. Durand, Phys. Rev. A **45**, R6969 (1992).
[34] L. M. Blinov, M. I. Barnik, H. Ohoka, M. Ozaki, N. M. Shtykov, and K. Yoshino, Eur. Phys. J. E **4**, 183 (2001).
[35] N. Terasawa, H. Monobe, K. Kiyohara, and Y. Shimizu, Chem. Commun. (Cambridge) **14**, 1678 (2003).
[36] A. V. Zakharov and R. Y. Dong, Phys. Rev. E **64**, 042701 (2001).
[37] L. T. Hung, M. Kimura, and T. Akahane, Jpn. J. Appl. Phys., Part 1 **44**, 932 (2005).
[38] Y. Abe, N. Tanaka, M. Kimura, and T. Akahane, in *Proceedings of the 11th International Display Workshops (IDW '04), Niigata, Japan, 2004*, p. 175.
[39] H. Sakamoto, R. Banshou, M. Kimura, and T. Akahane, in *Abstracts of the 21st International Liquid Crystal Conference, Keystone, Colorado, USA, 2006*, p. 971.
[40] M. Kléman and C. Williams, Philos. Mag. **28**, 725 (1973).
[41] G. Porte, J. Phys. (Paris) **37**, 1245 (1976).
[42] R. Barberi, I. Dozov, M. Giocondo, M. Iovane, Ph. Martinot-Lagarde, D. Stoenescu, S. Tonchev, and L. V. Tsonev, Eur. Phys. J. B **6**, 83 (1998).
[43] O. O. Ramdane, P. Auroy, S. Forget, E. Raspaud, Ph. Martinot-Lagarde, and I. Dozov, Phys. Rev. Lett. **84**, 3871 (2000).
[44] A. Sparavigna, Recent Res. Dev. Appl. Phys. **4**, 91 (2001).
[45] A. Romanenko, I. Pinkevich, V. Reshetnyak, I. Dozov, and D. Stoenescu, Functional Mater. **12**, 97 (2005).
[46] Y. Toko, B. Y. Zhang, T. Sugiyama, K. Katoh, and T. Akahane, Mol. Cryst. Liq. Cryst. Sci. Technol., Sect. A **304**, 1985 (1997).
[47] Y. Toko, E. Shiba, T. Sugiyama, K. Katoh, and T. Akahane, Mol. Cryst. Liq. Cryst. Sci. Technol., Sect. A **316**, 227 (1998).
[48] G. Baur, W. Wittwer, and D. W. Berreman, Phys. Lett. **56**, 142 (1976).
[49] F. Nakano, M. Isogai, and M. Sato, Jpn. J. Appl. Phys. **19**, 2013 (1980).
[50] T. J. Scheffer and J. Nehring, J. Appl. Phys. **48**, 1783 (1977).
[51] A. Dyadyusha, A. Khizhnyak, T. Marusii, Yu. Reznikov, O. Yaroshchuk, V. Reshetnyak, W. Park, S. Kwon, H. Shin, and D. Kang, Mol. Cryst. Liq. Cryst. Sci. Technol., Sect. A **263**, 2331 (1995).
[52] D. W. Berreman, J. Opt. Soc. Am. **62**, 502 (1972).
[53] G. Porte, J. Phys. (Paris) **38**, 509 (1977).